STM JOURNALS

Research & Reviews: Journal of Physics
ISSN: 2278-2265(online), ISSN: 2347-9973(print)
Volume 5, Issue 1
www.stmjournals.com

Structural and Electrical Characterization of Mn-Zn Substituted $CaSr_2$: W-Type Hexaferrite

A.K. Akant[1]*, C.L. Khobaragade[2]

[1]Department of Physics, Manoharbhai Patel Institute of Engineering and Technology, Gondia, Maharashtra, India

[2]Department of Physics, Govindrao Wanjari College of Engineering, Nagpur, Maharashtra, India

Abstract

In the present investigation the samples with chemical composition $CaSr_2(Mn\text{-}Zn)_{x/2}Fe_{16-x}O_{27}$ (x= 0.2, 0.4, 0.6, 0.8, 1.0) have been synthesized by using chemical co-precipitation method. X-ray diffraction (XRD) and transmission electron microscopy (TEM) were used to study structure, lattice constants, crystallites size, x-ray density, bulk density, porosity and shape of ferrite powders. The prepared samples were found to have W-type hexagonal structure with the lattice parameters a= (5.77 Å–5.82 Å) and c= (33.08–33.47 Å). The average crystallites size calculated from XRD analysis is found to be 27.9 nm. The dependence of conductivity, dielectric constant and dielectric loss tangent on both the frequency and temperature was studied by using impedance analyzer. The increase in conductivity with an increase in temperature shows a semiconducting behavior of the compound. The room temperature (RT) resistivity varies from $5.38x10^5\Omega$-cm to $1.43x10^8\Omega$-cm with the doping concentration.

Keywords: *XRD, VSM, electrical properties, hysteresis*

****Author for Correspondence*** E-mail: akakant@gmail.com

INTRODUCTION

Hexagonal ferrites have been a topic of interest due to their high resistivity and low eddy current losses [1–8]. Due to their low eddy current losses, there exist no other materials with such a wide ranging value to electronic applications in the terms of power generation, conditioning and conversion. There are six types of hexagonal ferrites, M-type ($AFe_{12}O_{19}$), W-type ($AMe_2Fe_{16}O_{27}$), Y-type ($AMe_2Fe_{12}O_{22}$), X-type ($A_2Me_2Fe_{28}O_{46}$), U-type ($A_4Me_2Fe_{36}O_{60}$) and Z-type ($A_2Me_2Fe_{24}O_{41}$). A W-type ferrite with chemical composition $AMe_2Fe_{16}O_{27}$, where 'A' represents alkali earth metals, usually Ba, Sr, Ca, Pb, etc. and Me represents a divalent metal ion, has same crystal structure as that of M-type ferrite except the structural 'R' blocks are separated by two 'S' blocks. The unit cell is composed of sequence RSSR*S*S*, where * represents rotation through 180° [9–13]. The presence of divalent and trivalent cations makes the W-type ferrites interesting for different technical application, since their characteristics may be varied by substitution of both divalent and trivalent cations. W-type hexaferrite are widely used in high density magnetic recording media, over coat-free, contact or semi-contact recording media and microwave tunable devices working at high frequency, above 70 GHz [14–17]. Method of synthesis plays an import role in controlling homogeneity, morphology and magnetic properties of hexagonal ferrites.

In the present work, a co-precipitation method was used to obtain homogeneous, ultra-fine and reproducible $CaSr_2(Mn\text{-}Zn)_{x/2}Fe_{16-x}O_{27}$ hexaferrites particles. This method is suitable for preparing particles in the nano range.

EXPERIMENTAL

$CaSr_2(Mn\text{-}Zn)_{x/2}Fe_{16-x}O_{27}$ hexaferrites particles were prepared by chemical co-precipitation method. AR grade calcium nitrate ($Ca(No_3)_2$), strontium nitrate ($Sr(No_3)_2$), manganese nitrate ($Mn(No_3)_4$), zinc nitrate ($Zn(No_3)_2$) and ferric nitrate ($Fe(No_3)_3.9H_2O$) were used as starting materials. Stoichiometric amounts of calcium nitrate, strontium nitrate, manganese nitrate, zinc nitrate and ferric nitrate were dissolved one by one in 100 ml of

distilled water. Ammonia solution (25%) was added slowly to adjust pH of 7. The mixed solution was stirred for two hours by using magnetic stirrer and was kept for 24 h for ageing. The calcium-strontium hexaferrite precipitate was separated in a centrifuge machine. The precipitate was washed in 1:1 mixture of methanol and acetone followed by 100% de-ionized water to remove impurity. The precipitate was dried at 100° C for about 24 hours and crushed and calcinated at 1000° C for 4 h. Finally, crushed for 5 h to obtained $CaSr_2$ $(Mn\text{-}Zn)_{x/2}Fe_{16\text{-}x}O_{27}$ hexaferrite particles.

The X-ray diffraction was studied by using XPERT-PRO diffractometer. The lattice parameters (a and c), x-ray density, bulk density, porosity and particle size were calculated from the XRD analysis. The microstructure was studied using transmission electron microscopy (TEM).

RESULTS AND DISCUSSION

Structural Characterization

The polycrystalline Mn-Zn doped $CaSr_2$: W-type ferrites were studies by the X-ray powder diffraction method (Figure 1) and found to exhibit a hexagonal W-type symmetry. The lattice parameters were calculated from the relation:

$$\frac{1}{d^2} = \frac{4(h^2 + k^2 + kh)}{3a^2} + \frac{l^2}{c^2}$$

The lattice parameters 'a' varies from 5.77–5.82 Å and 'c' varies from 33.08–33.47 Å. From structural parameters characterized by lattice constants 'a' and 'c' (Table 1), it becomes clear that lattice constant 'a' shows less variation and that of 'c' increases with substitution. This is in agreement with the fact that all hexagonal ferrites exhibit constant lattice parameter 'a' and variable parameter 'c' [18].

The increase in c values may be attributed to the larger ionic radii of Mn (0.67 Å) and Zn (0.74 Å) than iron (0.64 Å).

The X-ray density (dx) is determined from the relation,

$$d_x = \frac{2M}{N\ 0.866a^2c}$$

Where, M is the molecular weight, N is an Avogadro's number, "a" and "c" are lattice constants. The variation in X-ray density may be due to the difference in the molecular mass of doped samples (Mn- 55 amu and Zn- 65 amu) and undoped sample (Fe- 56 amu) [19].
The porosity (P) is calculated from the relation:

$$P = 1 - \frac{d}{d_x}$$

Where, d is bulk density and dx is X-ray density.

The crystallite size (D) is determined by using Debye-Scherrer formula as under [20, 21]:

$$D = \frac{0.9\lambda}{b\cos\theta}$$

Where λ is the wavelength and b is the broadening of diffraction line measured at half-width of maximum intensity (FWHM). The lattice parameters, unit cell volume, crystallite size, x-ray density, bulk density and porosity are shown in Table 1.

The transmission electron micrograph (TEM) for three samples (x= 0.2, 0.4, 0.6) are shown in Figure 2. The average crystallite size is found to be 27.9 nm, which agrees nearly with the crystallite size obtained from XRD analysis (Table 1).

Table 1: *Lattice Parameters "a" &"c", Unit CELL volume, Crystallite Size, X-ray Density, Bulk Density and Porosity.*

Mn-Zn Conc.	a (Å)	c (Å)	Volume ($Å^3$)	c/a	D (nm)	dx (g/cm^3)	d (g/cm^3)	P
0.0	5.82	33.08	970.7106	5.68	47.67	5.27	2.95	0.44
0.2	5.81	33.10	967.8354	5.70	33.84	5.29	3.06	0.42
0.4	5.79	33.18	962.0763	5.73	36.02	5.32	3.11	0.42
0.6	5.78	33.23	961.5826	5.75	40.18	5.33	3.20	0.40
0.8	5.80	33.23	966.8134	5.73	48.01	5.30	3.30	0.38
1.0	5.77	33.48	966.6402	5.80	41.18	5.31	3.08	0.42

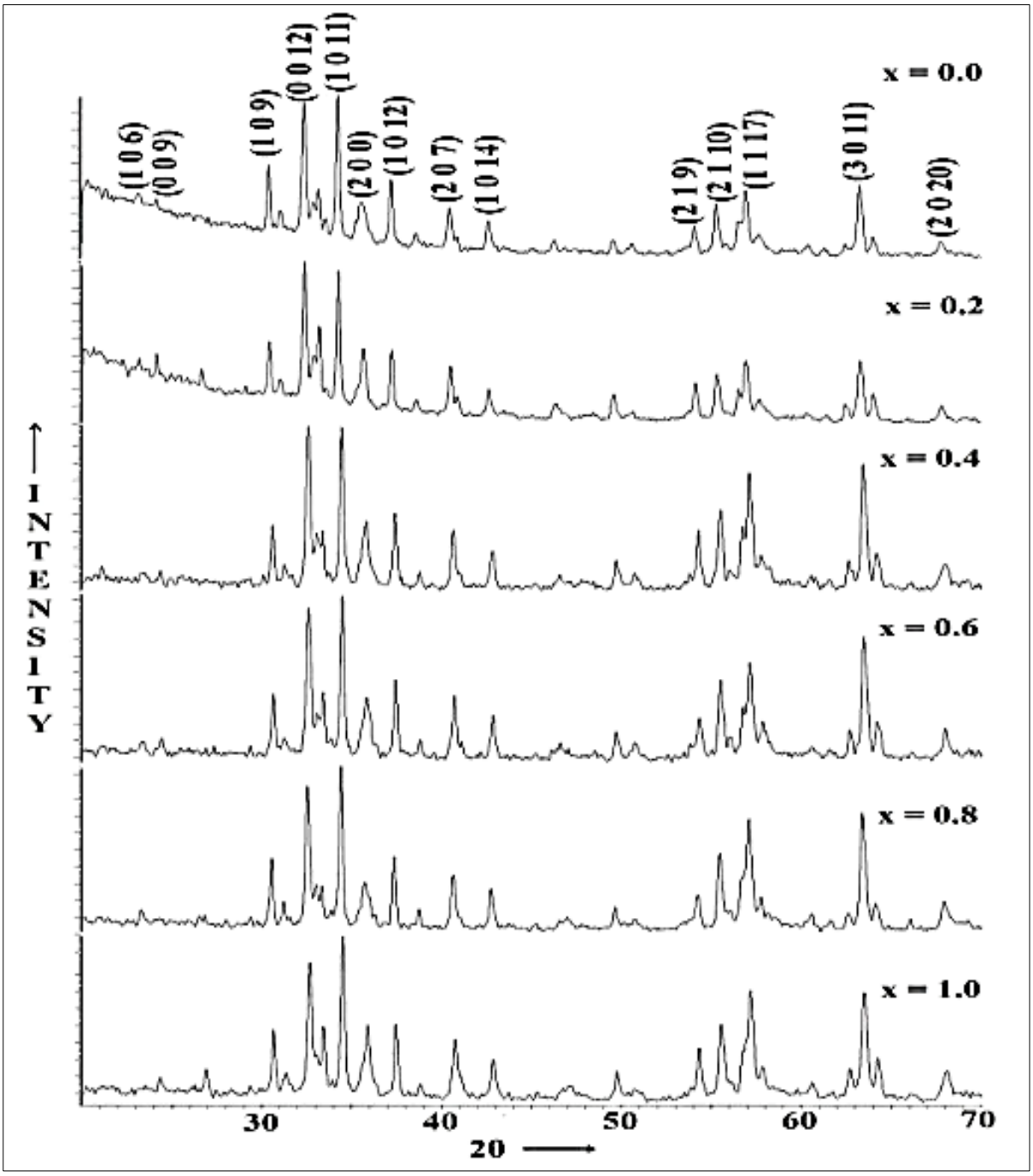

Fig. 1: *XRD of $CaSr_2(Mn\text{-}Zn)_{x/2}Fe_{16-x}O_{27}$.*

Electrical Properties

The variation of conductivity with temperature is shown in Figure 3. As expected, the conductivity increases with temperature showing semiconductor behavior of the material. It can be seen that log σ increases with that of temperature according to the Arrhenius equation; $\sigma = \sigma_0 exp\left(\frac{-E}{kT}\right)$, where E is the activation energy, k is Boltzmann's constant and T is absolute temperature [8]. For each sample, there are two regions characterized by transition temperature and having different slopes. This is a magnetic transition from ferromagnetic to paramagnetic. The transition temperature is found to decrease with the Mn-Zn concentration. The activation energy increases on passing through the transition temperature (Table 2). It may be due to valence exchange mechanism between Fe^{+3} and Fe^{+2} [22].

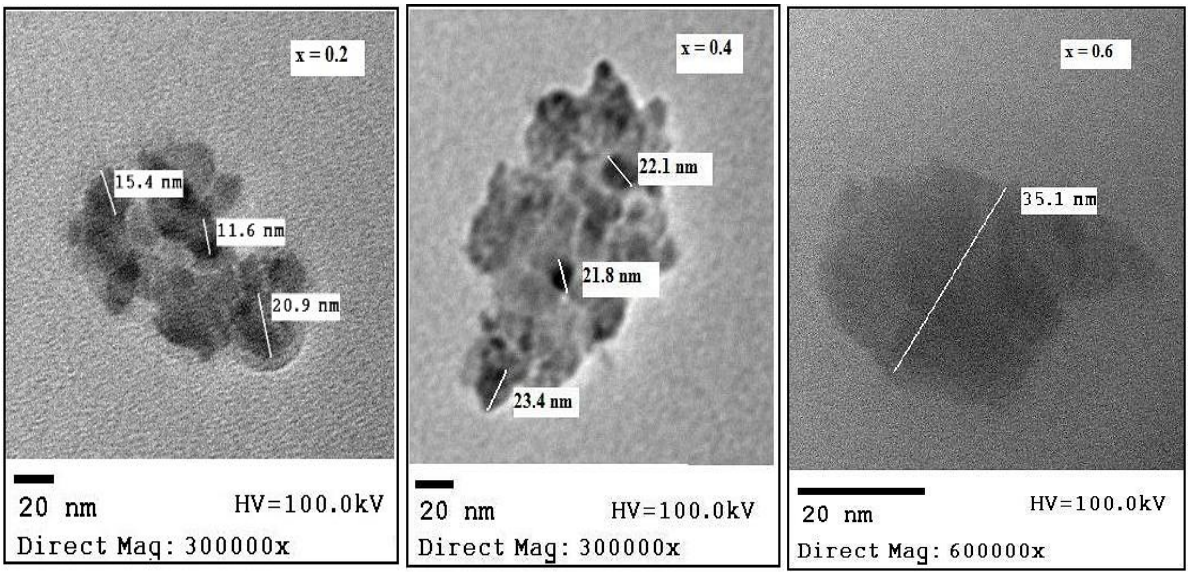

(a) *(b)* *(c)*

Fig. 2: *TEM Images for (a) x= 0.2, (b) x= 0.4, (c) x= 0.6*

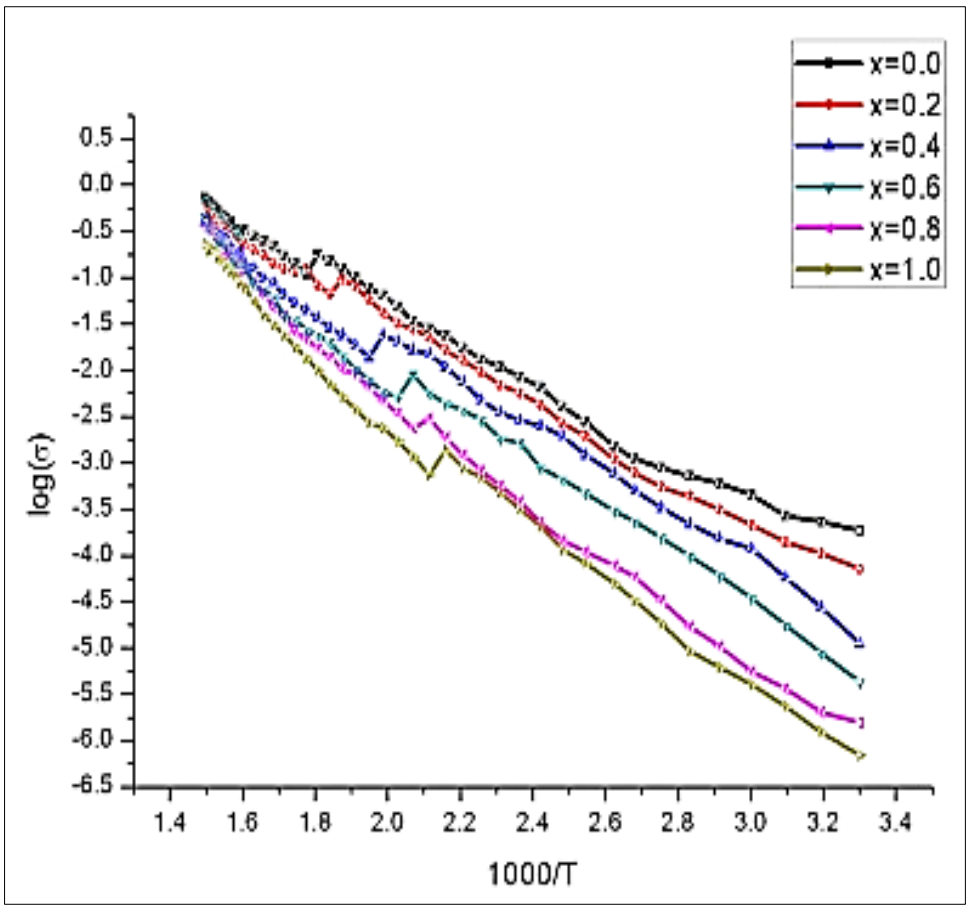

Fig. 3: *1000/T vs. log σ.*

Also an increase in the activation energy with the Mn-Zn concentration is due to increase in resistivity. The transition temperature is found to be nearly equal to curie temperature. The frequency dependence of dielectric constant (ϵ) and dielectric loss tangent (tan δ) is shown in Figure 4. The dielectric constant decreases with the increasing frequency.

According to Koops model, the high values of the dielectric constant at low frequencies can be attributed to the interfacial space-charge

polarization which arises from the heterogeneous structure of the samples, where ferrites samples can be considered as consisting of well conducting grains separated by poorly conducting grain boundaries [23, 24]. The loss tangent decreases with increasing frequency as expected [25]. Since the dielectric loss tangent depends on the ability of charges to follow the external applied electric field, the decrease of tan δ with increasing frequency is due to the fact that the polarization cannot follow the changes of external field beyond a certain frequency [23].

Table 2: *Activation Energy and Transition Temperature.*

Conc.	Activation energy (eV)		Room Temperature Resistivity (Ω - cm)	Transition temperature (K)	Curie temperature (K)
	Ferri	Para			
0.0	0.382	0.476	5.38E+05	552.99	561
0.2	0.389	0.467	1.40E+06	533	529
0.4	0.423	0.557	9.02E+06	503	500
0.6	0.448	0.628	2.32E+07	483	478
0.8	0.483	0.662	6.41E+07	473	470
1.0	0.505	0.705	1.43E+08	462.99	462

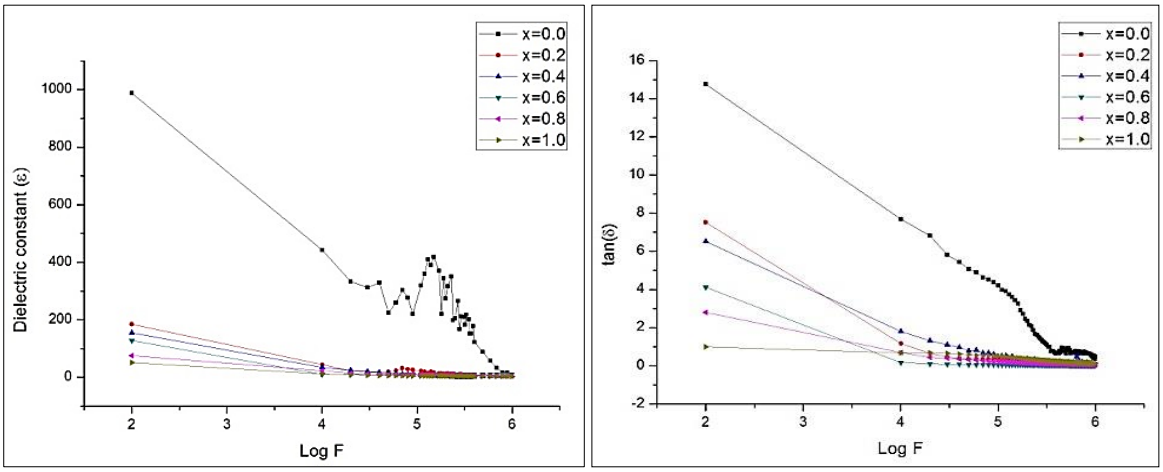

(a) *(b)*

Fig. 4: *Frequency Dependence of (a) Dielectric Constant (b) Loss Tangent.*

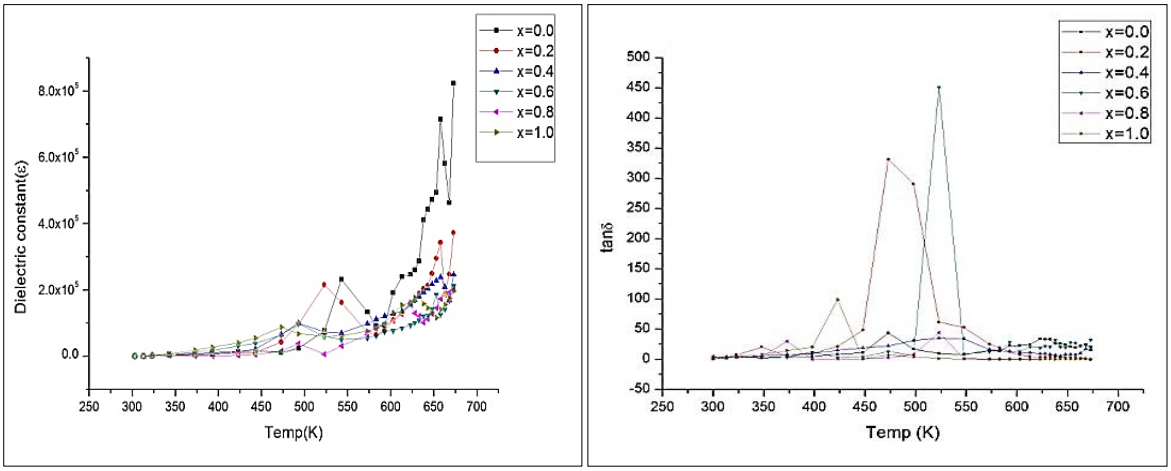

(a) *(b)*

Fig. 5: *Temperature Dependence of (a) Dielectric Constant (b) Loss Tangent.*

The temperature dependence of dielectric constant and dielectric loss tangent is shown in Figure 5. The dielectric constant increases with temperature showing a maximum at nearly transition temperature. The dielectric loss tangent initially increases with temperature and then decreases. The increase of tan δ with increasing temperature may be due to increase of the hopping frequency of the charge carriers [23].

CONCLUSIONS

Nanocrystalline $CaSr_2Fe_{16}O_{27}$ hexaferrite powders were synthesized successfully by co-precipitation method. The single domain particles of W- type hexaferrite were obtained at 1000° C. The X-ray diffraction patterns confirm that W-hexagonal phase is dominant. However, in some samples, few extra peaks corresponding to M- type were also observed. The crystallite size, as obtained from XRD analysis, varies from 33.84–48.01 nm. The electrical conductivity increases with temperature indicating semiconducting behavior of material. The dielectric constant and loss tangent decreases with frequency of applied electric field.

The high values of dielectric constant at low frequencies are due to the interfacial polarization ensuring that the samples can be considered as formed of well conducting grains and poorly conducting grain boundaries in agreement with Maxwell-Wagner theory with Koop's model.

ACKNOWLEDGEMENT

Author is thankful to Tata Institute of Fundamental Research (TIFR), Mumbai, Maharashtra, India,

REFERENCES

1. Mukhtar A, Ihasn A, Islam MU, et al. Effect of sintering temperature on magnetic and electrical properties of nano-sized Co_2W- hexaferrites. *Cer. Int.* 2012; 38; 1267–1273p.
2. Vishwanatha B, Murthy VRK. *Ferrite Materials.* New Delhi U.P. Narosa Publishing House; 1990.
3. Snelling EC. Soft Ferrites/Properties and Application. Second Edn. London: Butter Worths; 1988.
4. Smith J, Wijn HPJ. *Ferrites.* Eindhoven: Philips Technical Library; 1959.
5. Morisako A, Matsumoto M, Naoe M, et al. The effect of oxygen gas pressure on Ba-ferrite sputtered films for perpendicular magnetic recording media. *IEEE Trans. Magn.* 1988; 24(6): 3024–3026p.
6. Hylton et al. Ba-ferrite thin film media for high-density longitudinal recording. *J. Appl. Phys*. 1994; 75; 5960–5965p.
7. Niesen TP, Guire MR. Deposition of ceramic thin films at low temperatures from aqueous solutions. *J. Electroceram.* 2001; 6(3): 169–207p.
8. M. EL-SAADAWY. Structural,Transport properties and diffusion study of oxygen atoms for Mn_2-W type hexaferrite doped with Cu^{2+}. *J. of Mat. Sci and Engg with Adv Tech.* 2012; 5:135–151p.
9. Ahmad et al. Synthesis and characterization of Al-substituted W-type hexagonal ferrites for high frequency applications. *J. of Ally and Comp*. 2013; 577: 382–388p.
10. Kumar et al. Cation distribution in mixed Mg-Mn ferrite systems from X-ray diffraction technique and saturation magnetization. *IJPAP*. 2006; 44: 930–934p.
11. Standley KJ. *Oxide Magnetic Materials.* Oxford; Clarendon Press. 1962; 36p.
12. ElKony et al. Dielectric behavior of Mg-Zn W-type hexaferrite. *Egypt. J. Sol*. 2000; 23(1): 137–146p.
13. Arjunwadkar R, Salunkhe MY, Dudhe CM, et al. Structural, Electrical and Magnetic study of $SrNi^{2+}(Li^{1+}Fe^{3+})_{0.5}Fe_{16}O_{27}$ Ferrite. *J of Solid State Physics*. 2013; 6p.
14. Rana MU, Islam MU, Qadri U, et al. Fabrication and Characterization of W-Type Hexaferrites. *Journal of Research (Science)*. 2006;17(4): 219–224p.
15. Muller R. Preparation of W-type hexaferrite particles by the glass crystallization method. *J. Magn and Magn Mater*. 1991;101: 230–232p.
16. Surig et al. Investigations on $Zn_{2-x}Co_x$ W-type hexaferrite powders at low temperatures by ferromagnetic resonance. *J. Magn and Magn Mater*. 1995;150: 270–276p.
17. Ahmed MA, Okasha N, Kershi RM, et al. Extraordinary role of rare-earth elements on the transport properties of barium W-

type hexaferrite. *Materials Chemistry and Physics*. 2009; 113: 196–201p.
18. Kojima H, Wohlfarth EP. *Ferromagnetic Materials.* North-Holland, Amsterdam; 1982; 3: 305p.
19. Khan et al. Role of Ce-Mn substitution on structural, electrical and magnetic properties of W-type strontium hexaferrites. *J. Allys and Comp*. 2011; 509: 8042–8046p.
20. Ali et al. Influence of dysprosium addition on the structural, morphological, electrical and magnetic properties of nano-crystalline W-type hexaferrites. *Bull. Mater. Sci*. 2015; 38(1): 1–5p.
21. Iqbal et al. Mosbauer and magnetic study of Mn, Zr and Cd substituted W-type hexaferrites prepared by co-precipitation method. *Mater. Res. Bull*. 2011; 46: 1980–1985p.
22. Heneda K, Kojima H. *Physica Status Solidi (A)*. 1971; 6: 256p.
23. Abo-el-Ata et al. Dielectric and magnetic permeability behavior of $BaCo_{2-x}Ni_xFe_{16}O_{27}$ W-type hexaferrites. *J. Magn and Magn Mater*. 1999; 204: 36–44p.
24. Yafen et al. Pr^{3+} substituted W-type bariun ferrite: Preparation and electromagnetic properties. *J. Magn and Magn Mater*. 2012; 324: 616–621p.
25. Inaam MA. Dielectric behavior of Nickel-Zinc dopped hexagonal W-type barium ferrite. *J. Al-Nahrain University*. 2012; 15(2):102–105p.

Cite this Article
A.K. Akant, C.L. Khobaragade. Structural and Electrical Characterization of Mn-Zn Substituted $CaSr_2$: W-Type Hexaferrite. *Research & Reviews: Journal of Physics.* 2016; 5(1): 11–17p.